Eur. Phys. J. B (2025) 98:61
https://doi.org/10.1140/epjb/s10051-025-00909-2

THE EUROPEAN PHYSICAL JOURNAL B

Regular Article - Solid State and Materials

Engineering optoelectronic properties of the Pb-free perovskite $FASiBr_{3-X}I_X$ (X = 0, 1, 2 or 3) for photovoltaic applications: first principle analysis

Youssef El Arfaoui[1,a], Mohammed Khenfouch[2], Nabil Habiballah[1], and Simone Giusepponi[3]

[1] Theoretical Physics and High Energy Laboratory (LPTHE), Department of Physics, Faculty of Science, Ibn Zohr University, Agadir, Morocco
[2] Materials, Electrical Systems, Energy and Environment Laboratory (LMS3E), Materials and Energy Engineering Group, Faculty of Applied Sciences, Department of Applied Physics, Ait Melloul, Ibn Zohr University, 86153 Agadir, Morocco
[3] TERIN-ICT Division, Italian National Agency for New Technologies, Energy and Sustainable Economic Development (ENEA), CR Casaccia, 00123 Rome, Italy

Received 30 May 2024 / Accepted 20 March 2025 / Published online 11 April 2025
© The Author(s) 2025

Abstract. Lead-free perovskites have become a potential candidate for the development of the photovoltaic field. Here, we explored the structural and optoelectronic characteristics of silicon-perovskite $FASiBr_{3-X}I_X$ ($X = 0, 1, 2$ or 3) for solar device applications. Density functional theory has been applied. The band structure shows that $FASiBr_3$ $FASiBr_2I$, $FASiBrI_2$ and $FASiI_3$ have a semiconductor nature with a direct band gap of (2.09 eV) (2.60 eV) PBE(HSE), (1.90 eV) (2.38 eV) PBE(HSE), (1.71 eV) (2.12 eV) PBE(HSE) and 1.60 eV (2.08) PBE(HSE), respectively. In addition, the studied perovskites also exhibited great optical properties including, high absorption; moreover, we showed that the substitution of Br by I in $FASiBr_3$ perovskite can considerably enhance the optical behavior. The dielectric function showed that the edge of absorption of Br-substituted I in $FASiBr_3$ perovskite was shifted towards the low energy zone (red-shift) compared to $FASiBr_3$. As a result, $FASiI_3$ experiences greater absorption capability than its $FASiBr_3$ counterpart. These analyses indicate that FASiI3 is the best candidate for use as a Pb-free material for perovskite solar cells.

1 Introduction

Recent advancements in solar cell technology have focused on improving efficiency, stability, and scalability. Among the different solar cell types, perovskite, silicon, and dye-sensitized solar cells (DSSCs) have drawn significant attention due to their unique properties and potential for wide applications. Perovskite solar cells (PSCs) are a leading area of research due to their high efficiency and potential for low-cost production. Studies explore the structural and compositional optimization of PSCs, yielding insights into maximizing light absorption and charge carrier transport [1, 2]. Another recent study emphasizes optical material improvements for PSC stability and efficiency enhancement [3]. Silicon solar cells (Si-SCs) remain the most established technology in the commercial market due to their durability and mature fabrication processes. However, improving efficiency without significantly raising costs remains a challenge. Efforts have been made to innovate within this technology. For instance, the studies by Basher et al. focus on advancements in material processing to enhance electron mobility and light-harvesting capabilities [4, 5]. Additional insights into silicon cell efficiency can be found in Ref. [6], which examines novel silicon structures. DSSCs offer a cost-effective alternative with flexibility and transparency features, making them suitable for applications in indoor and low-light environments. Studies such as [7, 8] provide an overview of material innovations that enhance the light absorption of dye molecules, as well as on the chemical stability and electron transport improvements in DSSCs.

Hybrid organic–inorganic perovskites (HOIPs) with the ABX_3 structure have attracted special attention from the academic community and industries because of their exceptional features and high efficiency in solar cells' applications [9, 10]. Perovskites showed remarkable optoelectronic characteristics, such as long electron and hole diffusion lengths and excellent light absorption [11]. $CH(NH_2)_2PbI_3$ was found to have a long carrier lifetime, excellent carrier mobility and direct band

Supplementary Information The online version contains supplementary material available at https://doi.org/10.1140/epjb/s10051-025-00909-2.

[a] e-mail: youssef.elarfaoui@edu.uiz.ac.ma (corresponding author)

gap of 1.47 eV [12, 13]. In addition, the $CH(NH_2)_2PbI_3$ showed higher stability than $CH3NH_3PbI_3$ [14]. Despite their success in photovoltaic applications, the largest parts of these perovskites that demonstrate excellent properties include Pb. An issue thus arises for the implementation of these materials in solar cells due to the toxicity of lead. Also, the material's instability towards heat and moisture is another issue. That limits the solar cell efficiency, which makes scaling up commercialization challenging [15, 16].

To explore for potentially Pb-free perovskite, previous investigations have sought to address the toxicity issue by substituting Pb with Sn or Ge in $FAPbI_3$ and $MAPbI_3$, and the suitability of Sn and Ge as Pb substitutes has been confirmed [10]. Moreover, inspecting the optoelectronic properties of materials can assist us in comprehending their behavior and revealing their potential applications [17]. For this reason, theoretical analyses based on DFT have inspected the physical characteristics of lead-halide perovskites for solar cells [18, 19], as well as non-leaded perovskites [20–22]. Recently, a study has focused on a family of 48 ABX_3 perovskite materials, where (A = FA, MA or Cs), (B = Sn, Ge or Si), (X = I, Br or Cl) within the $DFT_{1/2}$ approach [23]. Furthermore, ab initio simulations have been done to explore a new ABX_3 structure for solar cells involving 90 ABX_3 candidates with FA, MA... as an A cation, Cd, Cu, Mg, as an B cations and [Cl, Br or I atoms as a X anions [24]. Also, in our previous work, to study perovskite materials for photovoltaic applications, DFT and SCAPS (Solar Cell Capacitance Simulator) software were applied [25–30].

High Efficient HOIPs based solar cells can be fabricated with the relatively less sophisticated solution-processed methods, lowering production costs. Nevertheless, there is still much room for improvement. As a means to improve light absorption, there is interest in the investigation of narrower band gap perovskites such as $FAPbI_3$. Sn-perovskites are studied to reduce the toxicity of Pb when replaced by much lower atomic number group IV elements (such as Sn); the situation gets worse, because of the reduction in stability of the divalent oxidation state for these elements. Silicon elements which play the most important role in modern industry, however, have received almost no attention in photovoltaic research community, and it has been reported that Silicon-based HOIPs does not possess a proper band gap for sunlight-harvesting. On the other hand, numerous emerging low-valent silicon materials, which are proven experimentally to be stable under the standard temperature and pressure [31–33], indicate the possibility of the existence of Silicon-based perovskites with excellent stability. Meanwhile, as reported in the previously, the hydrogen bonding in HOIPs tends to limit the oxidation of Sn^{2+}, thus the existence of strong hydrogen bonding is also expect to enhance the thermal stability of HOIPs with smaller group IV elements [34]. The discovery of Silicon-based perovskite not only contributes to the achievement of a novel narrow band gap perovskite for approaching the Shockley–Queisser efficiency limit [35] and an excellent optical absorption, but also deals with the environmental issues and economic sustainability concerns in the photovoltaic research community, mainly caused by toxic elements. This drawback prevents the wide use and commercialization of these materials. Therefore, further efforts are required to avoid this issue in the PSCs. In addition, all-inorganic perovskites are seen as a suitable alternative to overcome the thermal instability caused by the organic molecule, but they often experience phase instability [36]. For this reason, one may verify that there is no single perovskite with the ideal properties for photovoltaic applications. Surpassing the toxicity and stability issues while maintaining high efficiency is challenging. One way of controlling these properties is by taking advantage of the high compositional and structural flexibility of the perovskite materials. Much focus has been placed on halide perovskites, recent studies have begun exploring alternative perovskite compositions that could offer enhanced stability and compatibility with existing silicon-based technologies. For instance, recent work has shown that the incorporation of silicon within perovskite structures can lead to improved absorption of light in the UV region. Also, this Si-perovskites are mechanically stable and anisotropic [37, 38]. Additionally, density functional theory (DFT) studies have provided key insights into the behavior of Si-based perovskites $SiSnO_3$ and $SiGeO_3$ and double perovskite Ca_2TiSiO_6, highlighting their potential for high-efficiency optoelectronic applications [38, 39]. According to their report, $SiSnO_3$ and $SiGeO_3$ are semiconductors. $SiSnO_3$ has an indirect (M–X) energy state gap of 2.4 eV, and $SiGeO_3$ has a direct (X–X) energy gap of 3.1 eV. Despite these advancements, further investigation into the specific structural and electronic characteristics of Si-based perovskites remains limited. Our work aims to address this gap by providing a comprehensive analysis of these properties, offering valuable insights into their potential in optoelectronic applications.

The quest for alternative materials in optoelectronic applications has brought perovskite materials into sharp focus due to their excellent electronic and optical properties. However, while much of the current research has centered on halide perovskites, the potential of Si-based perovskites remains largely unexplored. The present study addresses this gap by providing a comprehensive (DFT) analysis of the structural, electronic, and optical properties of Si-based perovskites. This work is unique in its focus on the integration of silicon, a well-established material in the semiconductor industry, within the perovskite framework. By investigating Si-based perovskites, our study aims to advance the understanding of their intrinsic properties, offering valuable insights into how these materials could be optimized for applications in photovoltaics and optoelectronics. This analysis not only enhances the foundational knowledge of Si-based perovskites but also sets the stage for future research that could leverage the compatibility of silicon in next-generation device architectures.

In this context, a theoretical analysis of novel Pb-free $FASiBr_{3-X}I_X$ ($X = 0$, 1, 2 or 3) properties was performed, using both computational approaches: DFT and TDDFT. The study of silicon-based perovskite $FASiI_3$ for its application in the PSC has not been reported [40]. Herein, we focused on the electronic properties. The studied perovskite shown to possess semiconductor behavior with a direct band gap, which is very appropriate for photovoltaic solar cells; hence, this study will provide important insight on the perovskite structure for novel lead-free perovskite solar cells. The aim of this study is to analyze and engineer the structural, electronic, and optical properties of silicon-based perovskites for photovoltaic applications using density functional theory (DFT). Specifically, the study focuses on exploring the structural stability of the compounds through the calculation of stability parameters. Additionally, it investigates the electronic properties by determining the band structure and density of states to identify band gap characteristics optimal for light absorption. The optical properties, such as absorption coefficients and dielectric functions, are analyzed to assess their suitability for energy conversion. Furthermore, material modifications and doping strategies are proposed to optimize the properties for enhanced photovoltaic performance. Unlike previously published works, which primarily emphasize traditional perovskite materials such as lead-based compounds, our research introduces silicon as a core component. This substitution addresses environmental concerns while exploring new material combinations. Moreover, these aspects distinguish our work from the referenced studies, which do not explore these silicon-based configurations or their tailored engineering for improved performance.

The organization of the manuscript is as follows: in Sect. 2, we present the methods details. Section 3 includes the results for $FASiBr_3$, $FASiBr_2I$, $FASiBrI_2$, and $FASiI_3$ perovskite divided into Sect. 3.1 structural characteristics, Sect. 3.2 electronic characteristics, Sect. 3.2.1 the band gap energy when including the SOC/HSE correction Sect. 3.3 optical characteristics, In Sect. 4, conclusions are covered.

2 Methods

We employed for all the calculations the first-principles DFT and TDDFT; both methods are implemented within Quantum Espresso which is an integrated suite of open-source computer codes for electronic-structure calculations and materials modeling at the nanoscale [41]. The Generalized Gradient Approximation (GGA) with Perdew–Burke–Ernzerhof (PBE) approach was used, and the hybrid functional Heyd–Scuseria–Ernzerhof HSE was employed as it is reported to estimate the band gap accurately. The ultra-soft pseudo-potentials were used to generate interactions between electrons and ions [42–45]. The dielectric function of the optical characteristics was determined using TDDFT using the norm conserving pseudopotentials [46]

The calculations with the spin–orbital coupling SOC effect are performed using the fully-relativistic pseudopotentials [47]. The k-points ($5 \times 5 \times 5$) was used to sample the Brillouin zone; the Monkhorst–Pack k-point pattern presents the Brillouin zone integration [48]. The cut-off energy value was fixed at 100 Ry. The convergence tolerance for the self-consistent field calculation was set at 10^{-6} Ry.

The crystal structures were relaxed by varying the atomic position, employing the Broyden–Fletcher–Goldfarb–Shanno (BFGS) [49]. In fact, the atomic positions were totally optimized until the forces and energies on each atom were less than 10^{-3} Ry/Bohr and 10^{-4} Ry, respectively.

3 Results and discussion

3.1 Structural characteristics of $FASiBr_{3-X}I_X$ (X = 0, 1, 2 or 3)

In this part, we focused on the optimization of $FASiBr_{3-X}I_X$ ($X = 0$, 1, 2 or 3) unit cell, which represents an important initial process in the numerical investigation. To inspect the properties of the material under investigation, the cubic structure (S.G: *Pm3̄m*, #221) was fixed for $FASiBr_{3-X}I_X$ ($X = 0$, 1, 2 or 3).

The unit cell includes 12 atoms, as shown in the illustration in Fig. 1, illustrated employing the VESTA software [27].

The Goldschmidt tolerance factor is frequently used as a metric for evaluating the potential formation of a perovskite structure, which expressed as:

$$t = \frac{r_A + r_X}{\sqrt{2}(r_B + r_X)}. \quad (1)$$

In this Eq. (1), r_A, r_B, and r_X stand for the ionic radii specific to the FA cation, the Si anion, and the Br anion. In general, perovskite structures are more inclined to develop when the tolerance factor value falls between $0.8 \leq t \leq 1.0$. In addition, perovskite structures with tolerance factors between 0.9 and 1.0 tend to presents a great structural soundness and stability. For $FASiBr_3$, the calculated tolerance factor is about 1.8 (where $r_A = 2.79$ Å, $r_B = 1.17$ Å, and $r_X = 1.33$ Å), indicating its acceptable structural stability. Another important geometric ratio is the octahedral factor O_f, [50] defined as

$$O_f = \frac{r_B}{r_X}.$$

This parameter is applied to evaluate the fit of the B cation into the respective halide X_6 octahedron. For a perfect cubic perovskites structure, the O_f should not be too small for structural stability and is suggested to

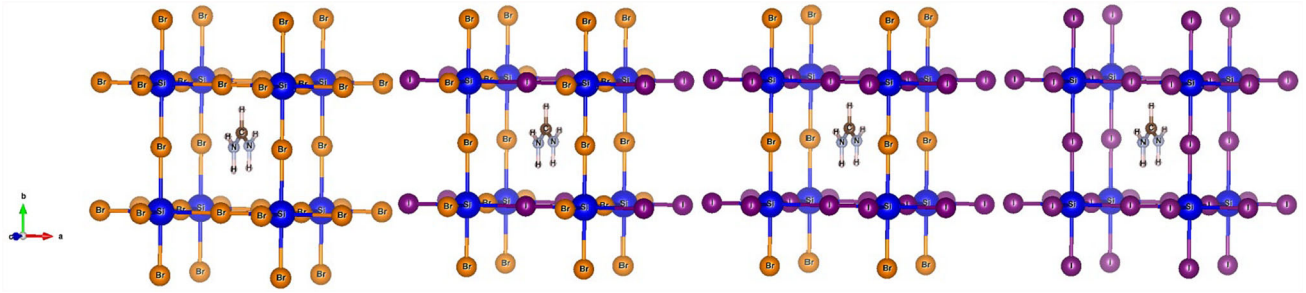


Fig. 1 Structure presentation of the cubic $FASiBr_{3-X}I_X$ ($X = 0$, 1, 2 or 3) perovskite employing the VESTA [27]

be better in the range from 0.4 to 0.8 [51]. The octahedral factor O_f of $FASiBr_3$ is found to be 0.87. The values of all Silicon-based perovskite are found to be smaller than the empirical criterion 0.4. However, seem not to sufficiently examine the stability of cubic perovskites structures, in which some perovskites were found to exist stable high dimensional network even their octahedral factor is too small, such as $MASiI_3$ ($O_f = 0.35$) and $FASiI_3$ ($Of = 0.30$) [52].

To perform the geometry optimization of the structural parameters of $FASiBr_{3-X}I_X$ ($X = 0$, 1, 2 or 3), the total energy of the studied perovskite has been calculated; in fact, the total energies of the $FASiBr_{3-X}I_X$ ($X = 0$, 1, 2 or 3) have been calculated for several lattice parameters 'a' (Å) with GGA-PBE approach, (see Fig. 2a–d). Our results of the total energy values of $FASiBr_{3-X}I_X$ ($X = 0$, 1, 2 or 3) as depend of the lattice parameter are illustrated in Fig. 2.

Indeed, Fig. 2a provides our findings for the FASiBr3, in addition, Fig. 2b presents the dependency of the total energy on the lattice parameter for $FASiBr_2I$, while, Fig. 2c, d illustrates the findings for $FASiBrI_2$ and $FASiI_3$, respectively. From these figures, it is found that the minimum total energy is positioned at $a = 6.2$ Å for the $FASiBr_3$ material. The minimum value is positioned at the lattice parameters $a = 6.3$ Å for $FASiBr_2I$, and $a = 6.4$ Å for $FASiBrI_2$ and $FASiI_3$.

It is also observed that there is an increasing trend in the lattice parameters for $FASiBr_{3-X}I_X$ ($X = 0$, 1, 2 or 3), when the level of I increases which is due to the larger ionic radii of I as compared to that of Br which observed in previous works [53–55]. The volume of the unit cell also increases more with the increase of I level.

Our calculated optimum 'a' with volumes for $FASiBr_{3-X}I_X$ ($X = 0$, 1, 2 or 3) perovskite using the GGA-PBE approach is summarized in Table 1. The obtained 'a' is also increased as a result of changing Br with I, from $FASiBr_3$ to $FASiI_3$. Moreover, the obtained total energy demonstrated that $FASiBr_3$ provides the structure that is more stable, while the less stable structure is $FASiI_3$ perovskite. It is seen from Table 1 that when the 'X' anion size (from Br to I) gets larger, the optimized lattice parameter increase due to the larger ionic size of I atom, this results are consistent with other related studies on various perovskite materials [54, 56].

3.2 Electronic properties of $FASiX_3$ (X = Br or I) perovskite

The electronic properties, in particular the band gap values of an absorber are crucial for photovoltaic solar cell due to the fact that it contribute to make the cell capable to absorb light photons and convert it into electricity effectively. To inspect the electronic properties of the $FASiBr_{3-X}I_X$ ($X = 0$, 1, 2 or 3) perovskite, we calculate and investigate the electronic characteristic of $FASiBr_{3-X}I_X$ ($X = 0$, 1, 2 or 3) when the GGA-PBE approximation is applied. We present the different band structures, the DOS, PDOS of $FASiBr_{3-X}I_X$ ($X = 0$, 1, 2 or 3) using this approximation. In fact, we provide our results for the perovskite, when 'a' = 6.2 Å, for the $FASiBr_3$ to compute and investigate the band structures, the DOS and PDOS. While, For the $FASiBr_2I$, $FASiBrI_2$ and $FASiI_3$, the optimal lattice parameter was selected: $a = 6.3$ Å, $a = 6.4$ Å and $a = 6.4$ Å, respectively.

We present in Fig. 3 our findings for $FASiX_3$ ($X =$ Br). In fact, Fig. 3a illustrates the band structure. This figure shows the semiconducting nature of this material. It is demonstrated that the band gap is 2.09 eV. Moreover, this figure clearly illustrates that BCB and TVB are located at *R-point*, which confirms the direct band gap nature of the material. Here, the required moving energy of an electron from the valence to the conduction band of a direct band gap perovskite is lower than an indirect band gap perovskite. This phenomenon is responsible for the excellent optoelectronic performance of a direct perovskite material. In addition, this match well with the results found for the silicon-based perovskite in Ref. [57]. Also, it is evident that the calculated band gap is quite comparable to that reported in the literature. In fact, computational results from other researchers demonstrated that the $FASiI_3$ band gap was between 0.8 eV and 2.0 eV, see Ref. [24], when performing a first principle calculations applying DFT approach within GGA-PBE + D2 approximation for a tetragonal phase. The band gap of $FASiBr_3$ is suitable for photovoltaic technology. Figure 3b illustrates the DOS and PDOS of $FASiBr_3$. It is observed that the conduction band minimum CBM is mainly created with a combination of Si and Br orbitals. While, the

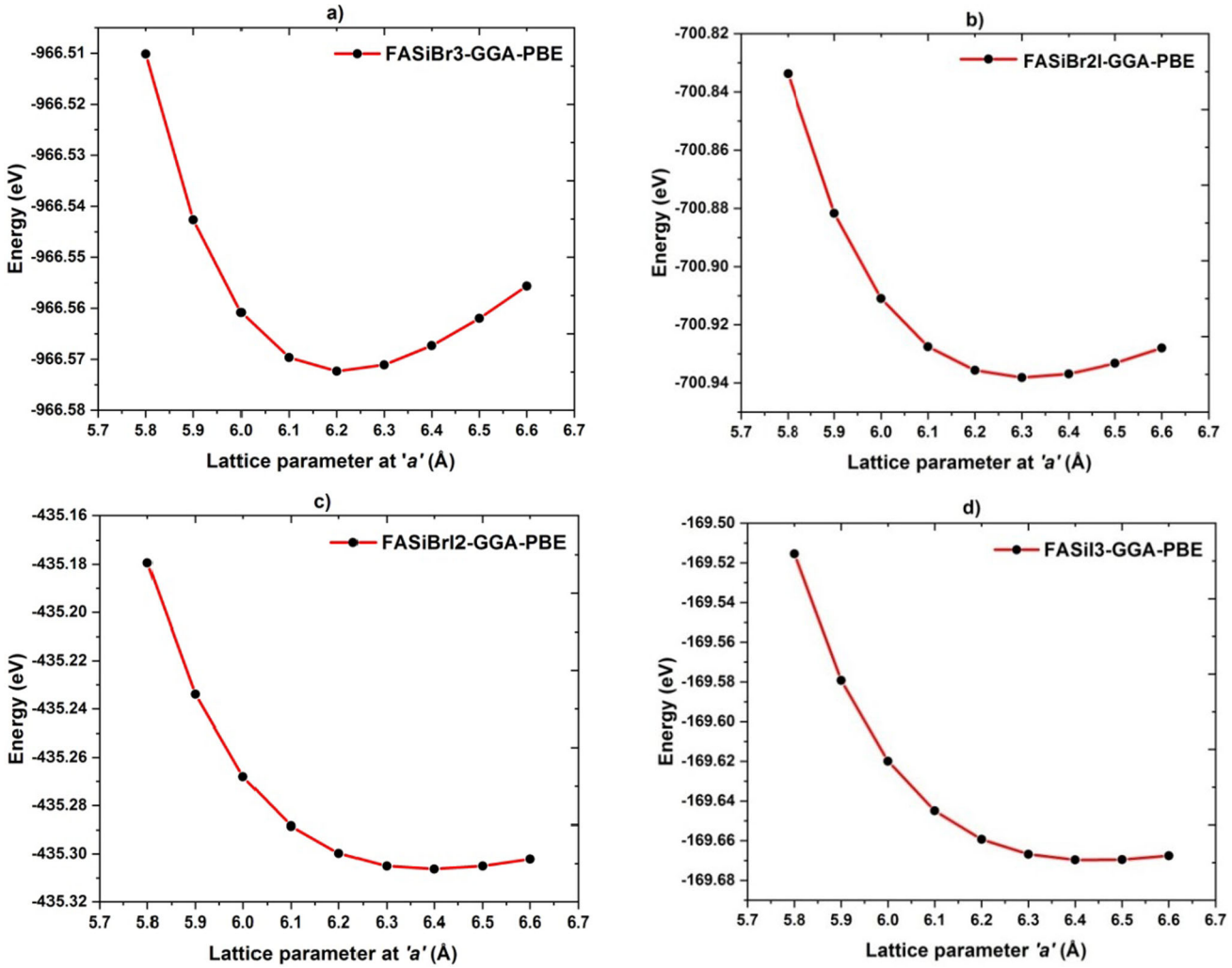


Fig. 2 The total energy of the $FASiBr_{3-X}I_X$ (X = 0, 1, 2 or 3) as a function of the lattice parameter, in **a** $FASiBr_3$, $FASiBr_2I$ in **b**, $FASiBrI_2$ in **c** and $FASiI_3$ in **d**

Table 1 The obtained optimum lattice parameters 'a' (Å), volumes 'V' (Å^3) and bulk modulus B of the cell unit of $FASiBr_{3-X}I_X$ (X = 0, 1, 2 or 3) perovskite material using GGA-PBE

Obtained results						
Lattice parameter a (Å)	$FASiBr_3$	6.20	Unit cell Volume 'V' in (Å^3)	238.32	Bulk modulus B in (GPa)	359.84
	$FASiBr_2I$	6.30		250.05		–
	$FASiBrI_2$	6.40		262.14		–
	$FASiI_3$	6.40		262.14		–
		6.34| [23]				
		6.30| [29]				

top of the valance band TVB is generated mainly with Br orbitals.

When varying the 'X' halogen to ($X = Br_2I$), the calculated band structure is presented in Fig. 4a. It is seen that the computed band gap is around 1.90 eV. Also, it was found that a significantly narrow band gap was calculated for this halogen mixture compared with $FASiBr_3$. On the other hand, Fig. 4b presents the density of states. It is found that Si, Br and I orbitals contribute the most to the generation of the BCB, While, the TVB is composed mainly of both Br and I orbitals. In 'FA' cation, the N atoms partially contributed to the valance band states within the structure. However, the other atoms presented minimal influence on the

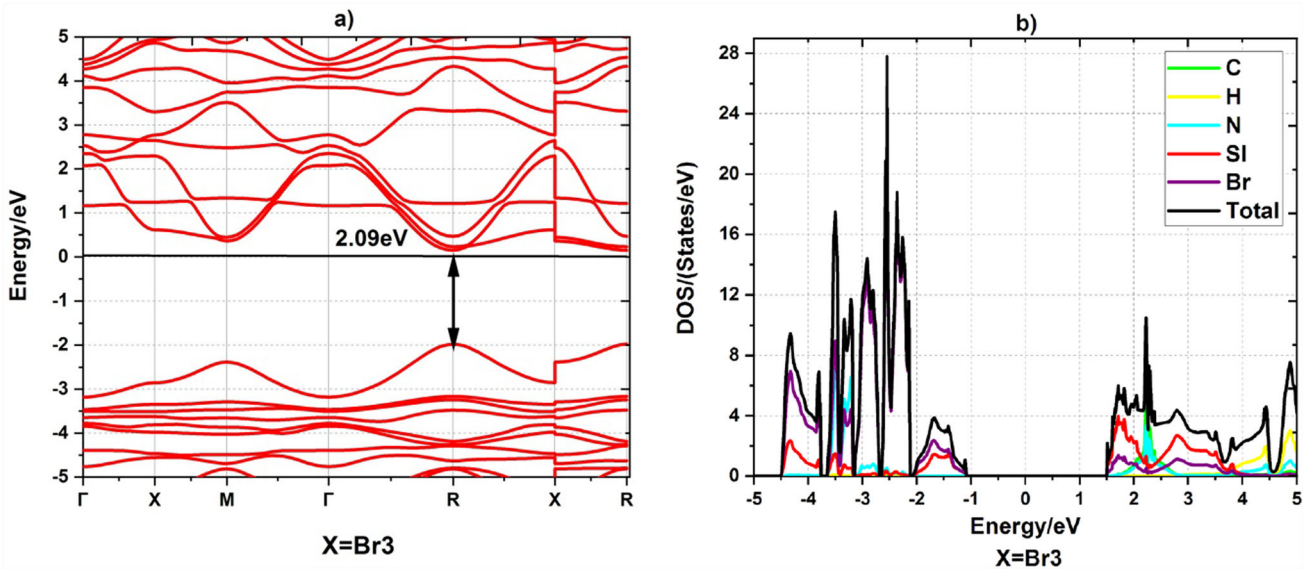


Fig. 3 **a** The band structure of $FASiX_3$ ($X = Br_3$), **b** the DOS and PDOS

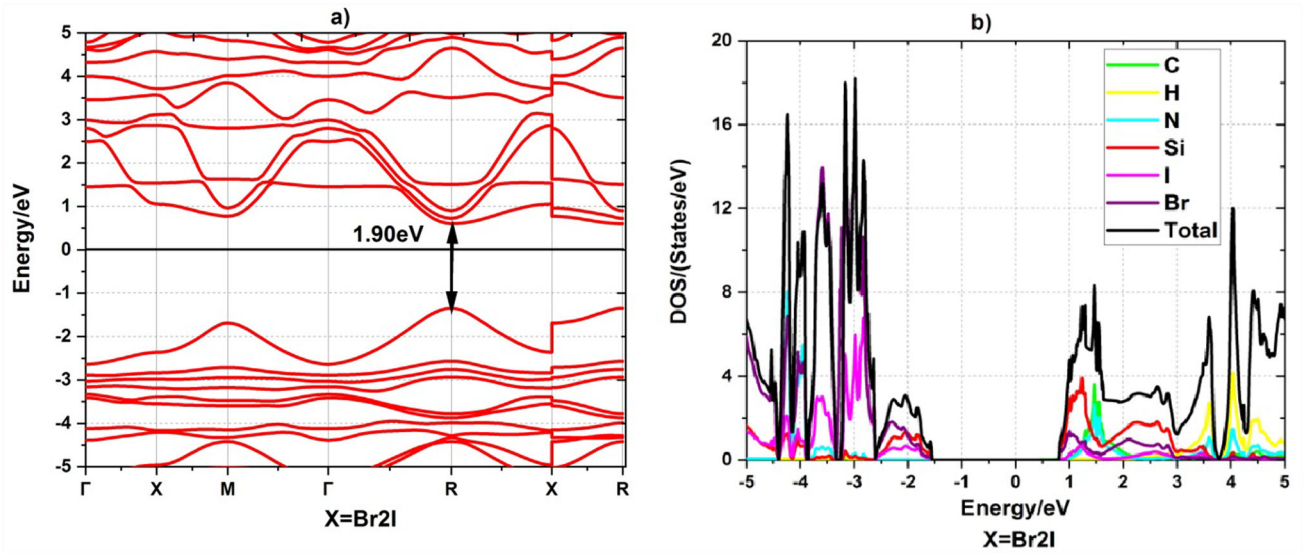


Fig. 4 **a** The band structure of the $FASiX_3$ ($X = Br_2I$) perovskite, **b** the DOS and PDOS

band edge. Significantly, the organic 'FA' cation does not directly contribute to the conduction or valence band; instead, it donates electrons to the perovskite. The orbitals of the 'FA' cation contribute to the energy zone far below the band gap edge. Several investigations have demonstrated that the orbitals of the organic cation 'A' of the ABX_3 perovskites have a minor effect on the conduction and valance band creation [58], which could indicate the insignificant effect of the organic element on the process of photon conversion [30].

The obtained findings for ($X = BrI_2$) have been illustrated in Fig. 5. The electronic properties are computed and plotted. The band structure is presented in Fig. 5a. The obtained band gap of $FASiBrI_2$ value is about 1.71 eV. It is generally recognized that the band gap for inorganic crystals is half-underestimated using the LDA approach [59]. Moreover, the DOS and PDOS of $FASiBrI_2$ are plotted in Fig. 5b. This figure shows that the BCB is composed of Si orbitals, and the TVB is created of the Si orbitals along with Br and I orbitals.

For ($X = I$), It is seen that the substitution of Br by an I atom decreases the energy of band gap. In fact, the band gap was obtained to be 1.60 eV for this Pb-Free FASiI3 perovskite,

This band gap was found to be around 0.66 eV in Ref. [23], using DFT with the GGA-PBE approximation and 1.39 eV using the $DFT_{-1/2}$ technique. As the band gap of FASiI3 moves to 1.1 eV, which represents the optimum band gap for single junction cells (SQ limit), this change in electronics properties caused by the substitution of the Br element can be useful to modify the band gap, allowing efficient single-junction solar devices [60].

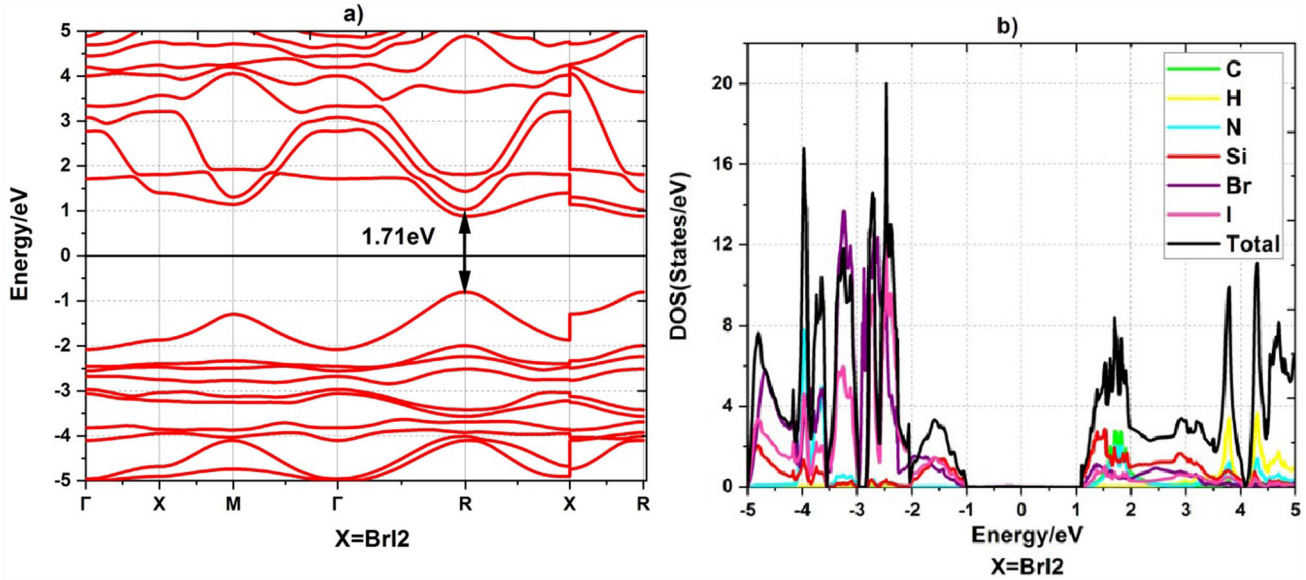


Fig. 5 **a** The band structure of the $FASiX_3$ ($X = BrI_2$) perovskite, **b** the DOS and PDOS

Table 2 The obtained band gap with GGA-PBE, HSE and HSE+ SOC approximations

	GGA-Pbe	HSE	HSE + SOC
$FASiBr_3$	2.09	2.60	2.52
$FASiBr_2I$	1.90	2.38	2.27
$FASiBrI_2$	1.71	2.12	1.97
$FASiI_3$	1.60	2.08	1.93
Other works	GGA-PBE + D2		GGA-PBE + SOC
	Between 0.80 eV and 2.00 eV [24]		0.90 eV [57]

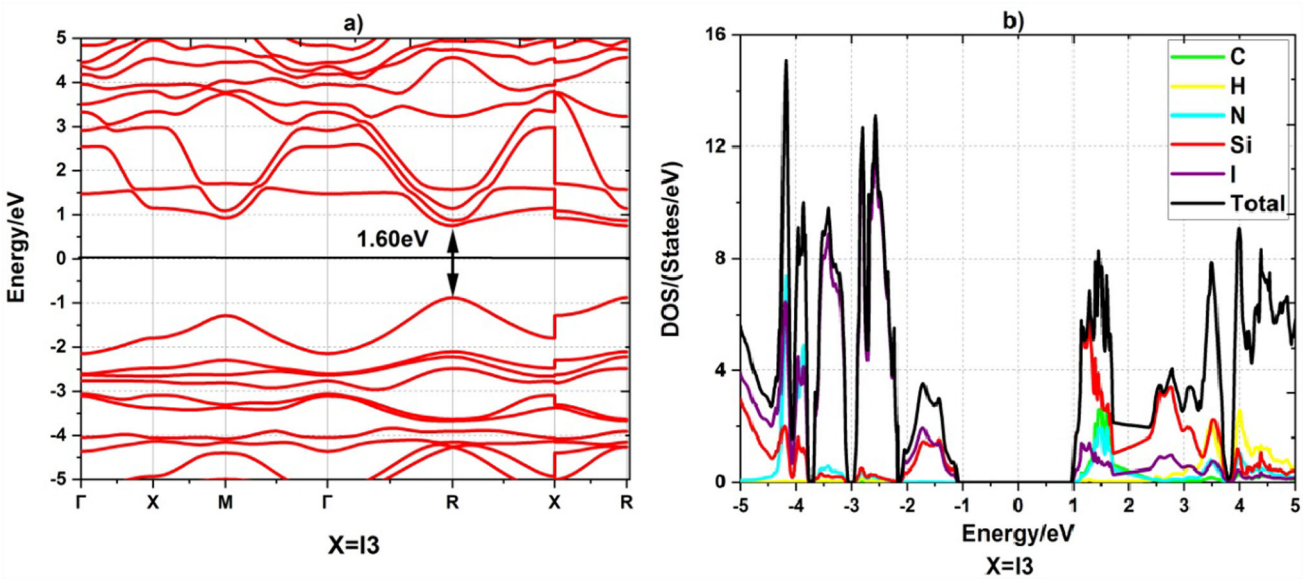


Fig. 6 **a** The band structure of the $FASiX_3$ ($X = I_3$), **b** the DOS and PDOS

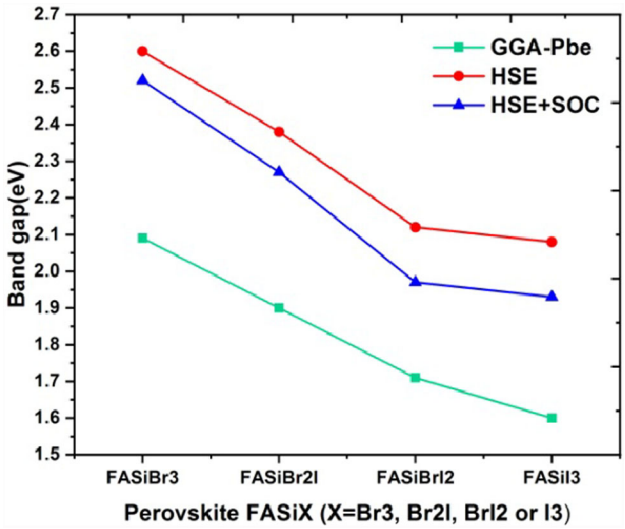


Fig. 7 Variation of calculated band gap of $FASiBr_{3-X}I_X$ ($X = 0$, 1, 2 or 3) using GGA-PBE, hybrid-HSE and HSE + SOC approximations

3.2.1 The impact of spin–orbit coupling and HSE approximation on the band gap

In this part, the electronic characteristics of the $FASiBr_{3-X}I_X$ ($X = 0$, 1, 2 or 3) perovskite when including SOC impact, have been inspected. Table 2 presents our computed band gap of $FASiBr_{3-X}I_X$ ($X = 0$, 1, 2 or 3) when applying GGA-PBE, HSE and HSE + SOC approximations. In addition, a comparison between our findings and those reported in previous results is presented in this table. It is observed that a Lower band gap was obtained when including the SOC correction into the HSE approximation; such findings of this decrease in band gap match well those of the literature (Fig. 6). The HSE approximation demonstrates that the $FASiI_3$ has a band gap of around 2.08 eV, and when the SOC is added, this band gap value decreases to reach 1.93 eV. Similarly, a band gap with the SOC was found in Ref. [57]. Moreover, the obtained band gap using GGA-PBE and HSE and HSE + SOC approximations was compared. The difference between the band gap calculated with HSE and HSE + SOC is 0.08 eV for $FASiBr_3$. It was observed that among the approximations, a reduced band gap was obtained when the GGA-Pbe approximation was applied and this value decreased as we moved from one perovskite to another: $FASiBr_3$, $FASiBr_2I$, $FASiBrI_2$ and $FASiI_3$. Figure 7 illustrates the variation of the band gap energy employing different approximations for the studied perovskites.

3.3 Optical characteristics of $FASiBr_{3-X}I_X$ (X = 0, 1, 2 or 3)

In this part, the optical properties of $FASiBr_{3-X}I_X$ ($X = 0$, 1, 2 or 3) are calculated using the complex dielectric function (Eq. 1), $\varepsilon_1(\omega)$ and $\varepsilon_2(\omega)$ are the real (Re) and imaginary (Im) term, respectively. The dielectric function can be obtained by employing the Kramer–Kronig relation [61], which is based on the light absorbed by the material and explains the mechanism of interaction of photon with electrons, when a system respond to an external radiation [11].

$$\varepsilon(\omega) = \varepsilon_1(\omega) + i\varepsilon_2(\omega). \tag{2}$$

Here, $\varepsilon_1(\omega)$ explains the light polarization and the dispersion of the incident photons within the material. The imaginary part describes the crystal's absorptive operation.

$$\varepsilon_1(\omega) = 1 + \frac{2}{\pi}\int_0^{\infty} \frac{\varepsilon_2(\omega')\omega' \mathrm{d}\omega'}{\omega'^2 - \omega^2}. \tag{3}$$

$\varepsilon_2(\omega)$, is related to the band structure that depends on the crystal's light absorption; which can be obtained employing the relation:

$$\varepsilon_2(\omega) = \frac{4\pi^2 e^2}{m^2\omega^2}\sum_{i,j} |\langle i|M|j\rangle|^2 (f_i(1-f_i)) \\ \delta(E_f - E_i - \hbar\omega)\mathrm{d}^3k. \tag{4}$$

The optical behavior of $FASiBr_{3-X}I_X$ ($X = 0$, 1, 2 or 3) in the excited state has been studied applying the time-dependent TDDFT by computing the imaginary and real elements $\varepsilon_2(\omega)$, $\varepsilon_1(\omega)$, respectively, as a dependent of the energy of the photon between 0 and 10 eV and Figs. 8, 9, 10, and 11 illustrate the findings.

The Im element $\varepsilon_2(\omega)$ which is related to the absorption of light in the crystal. Figures 8–9–10–11a illustrate the results after applying the GGA-PBE. In the Im term of $\varepsilon(\omega)$, this material experienced a very sharp peak in the low energy portion, it is observed the presence of a high peaks at photon energy about 5.6 eV for $FASiBr_3$ and 5.54 eV for $FASiI_3$. Moreover, $\varepsilon_2(\omega)$ ultimately exhibited a positive imaginary term, which demonstrated the semiconductor nature of the crystal. Clearly, $\varepsilon_2(\omega)$ increases and has strong peaks after

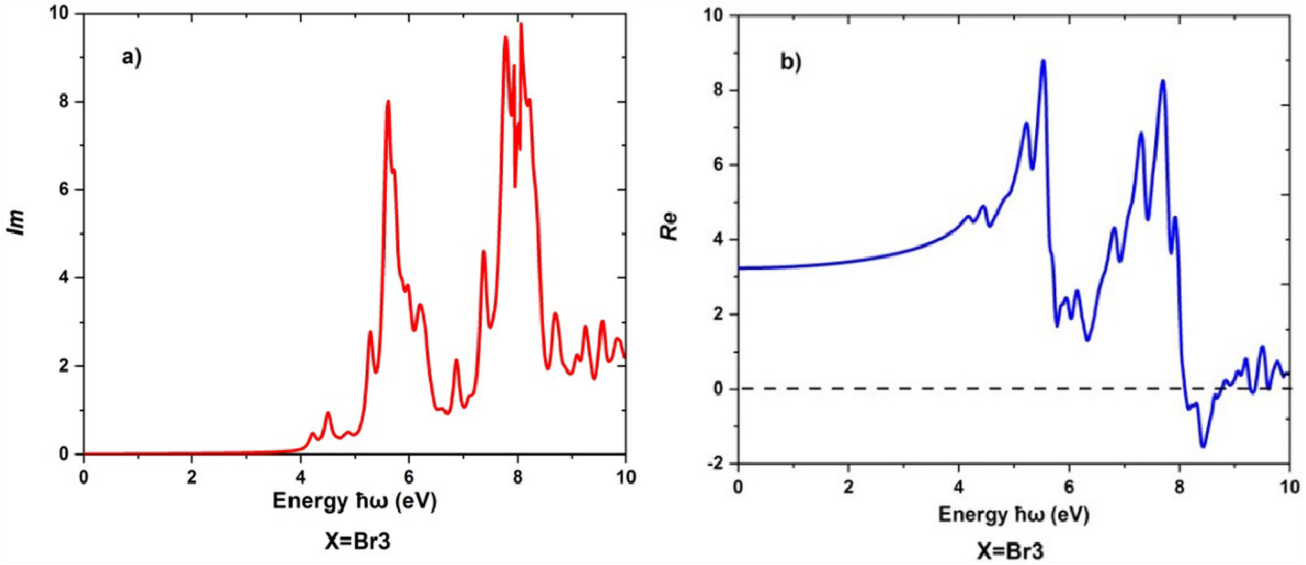


Fig. 8 In **a** the imaginary and **b** the real element of the dielectric function for $X = Br_3$

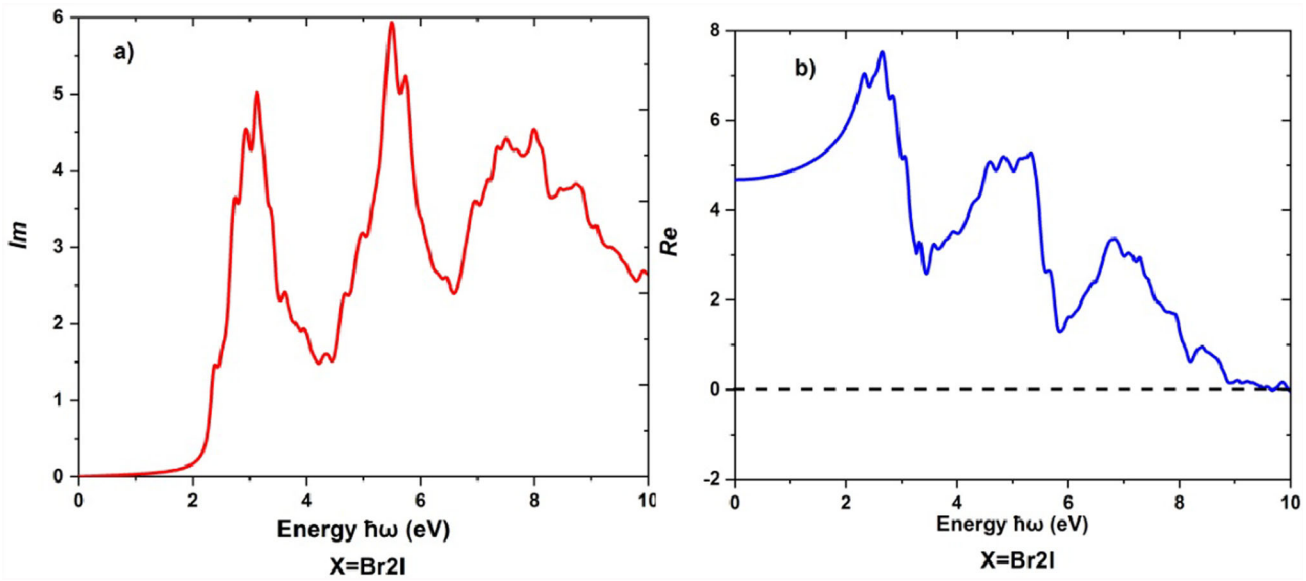


Fig. 9 In **a** the imaginary and **b** the real element of the dielectric function for $X = Br_2I$

photon energy 4 eV, demonstrating the high absorption of incident light. In addition, among the calculated imaginary elements of the four perovskites, the $FASiI_3$ magnitudes were higher than those of the $FASiBr_3$, $FASiBr_2I$ and $FASiBrI_2$ materials.

The dielectric constant of a material represents an essential parameter that provides important insight into the charge-recombination process and, as a results, the optoelectronic performance of the material [62]. A crystal with a great dielectric constant means that it has less charge-carrier recombination, and as a result, the efficiency of the solar cell will be increased. While crystals with a wider band gap exhibit a lower dielectric constant [63]. Here, $FASiI_3$ revealed a higher value of dielectric constants than $FASiBr_3$ as the band gap was reduced (as illustrated in the electronic structure) after changing Br with I.

For the real *Re* element of $FASiBr_{3-X}I_X$ ($X = 0$, 1, 2 or 3) perovskite, from Figs. 8–9–10–11b, it is shown that as the photons energy is at low values (there is no incident photon), the magnitude of $\varepsilon_1(\omega)$ is around zero, until the incident photon energy reaches the value of the optical band gap of perovskite, after this value, there is a transition from the interaction of incident light and the crystal free electrons that happen between the valence and conduction bands. In addition, the real element of $FASiI_3$ reached zero in the high-energy region (around 6.56 eV). This result suggests the transparency of $FASiI_3$ and hence the low absorption of photons with high energy. Indeed, the negative values in $\varepsilon_1(\omega)$ of the Re element represent reflection of light on

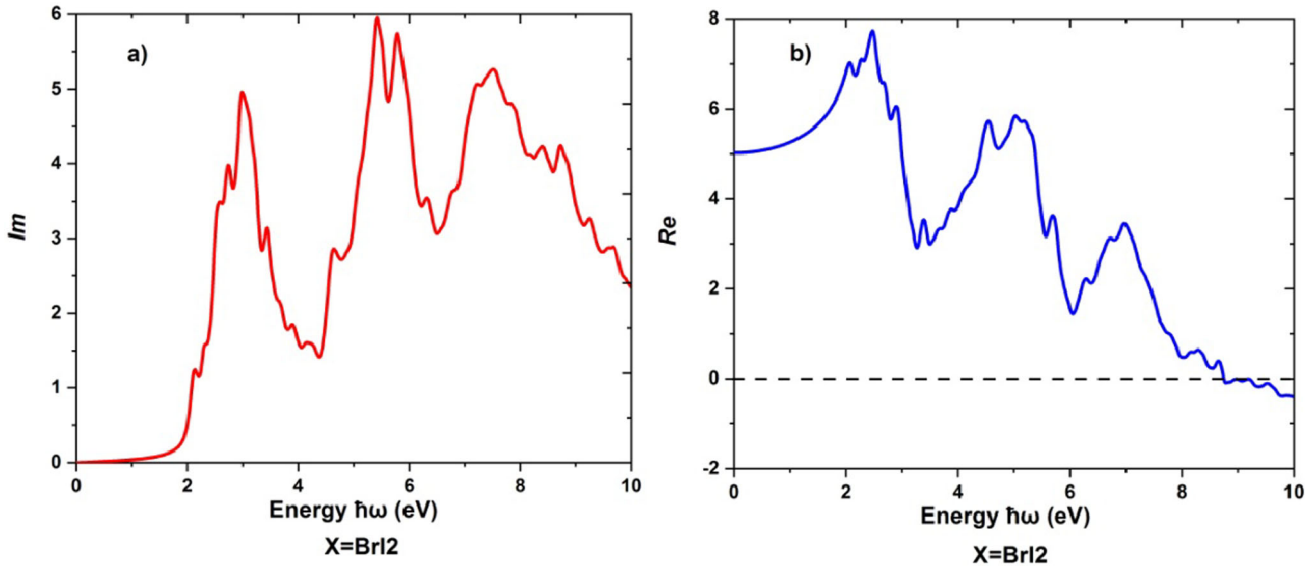


Fig. 10 In **a** the imaginary and **b** the real element of the dielectric function for $X = BrI_2$

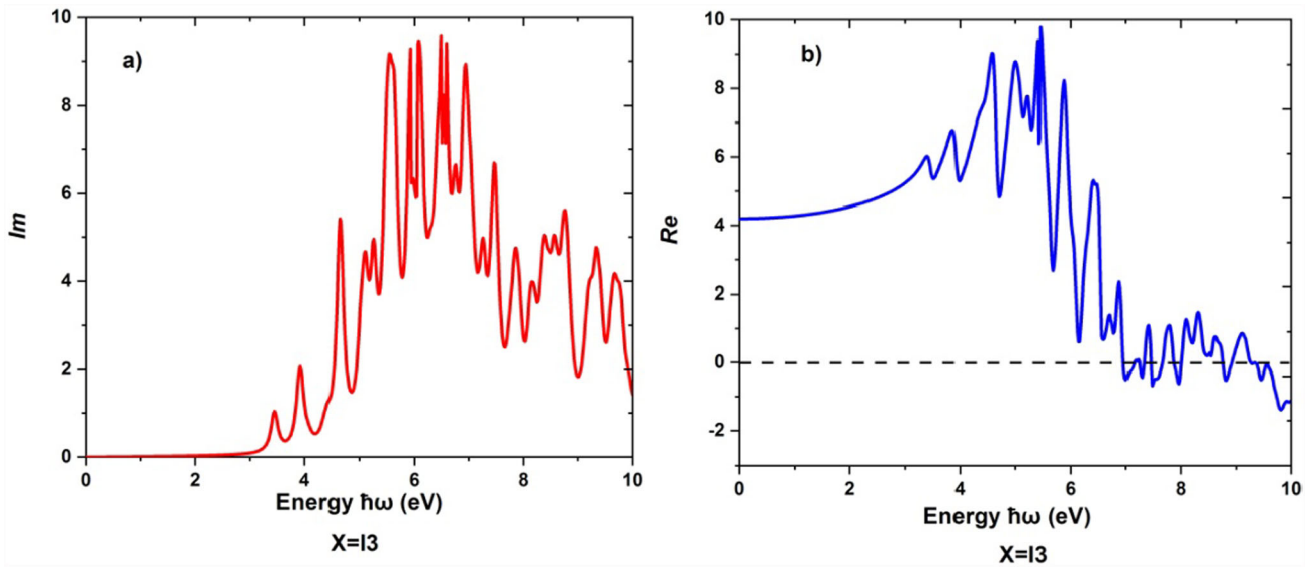


Fig. 11 In **a** the imaginary and **b** the real element of the dielectric function for $X = I_3$

the surface of perovskite which indicates the metallic behavior of the material.

Similar findings of the Re and Im elements for others Pb-free perovskites have been found in Ref. [64]. These findings above demonstrate that $FASiI_3$ perovskite material possessed an appropriate band gap for solar devices, also exhibited enough light absorption ability, making this material a potential candidate for PSCs.

The absorption coefficient of $FASiX_3$ is an essential factor since it determines the ability of the material to absorb light energy, providing valuable insight about its potential for photovoltaic application. The absorption coefficient of $FASiX_3$ is impacted by several parameters including crystal structure and thickness of the perovskite. The absorption coefficient spectra of $FASiX_3$ exhibits similar behavior to that of the imaginary part of the dielectric function. Figure 12a displays the absorption coefficient of $FASiX_3$ perovskite as a function of wavelength. It is clear that as the halogen atom moved from I to Br to I, the absorption peak of $FASiX_3$ exhibits a significant blue-shift. Also, absorption reveals consistent increases in optical absorption as energy increases. The absorption spectra demonstrate that all four materials display a maximum peak at around 160 nm, with $FASiI_3$ exhibiting the highest magnitude among the studied compounds. The results highlights that the $FASiI_3$ perovskite material exhibits the highest maximum absorption compared to $FASiBr_3$, $FASiBr_2I$ and $FASiBrI_2$ perovskites.

To complete the analysis of the optical properties, reflectivity is also known as an important optical parameter for judging the performance of an absorber in solar cells. The reflectance of perovskite materials

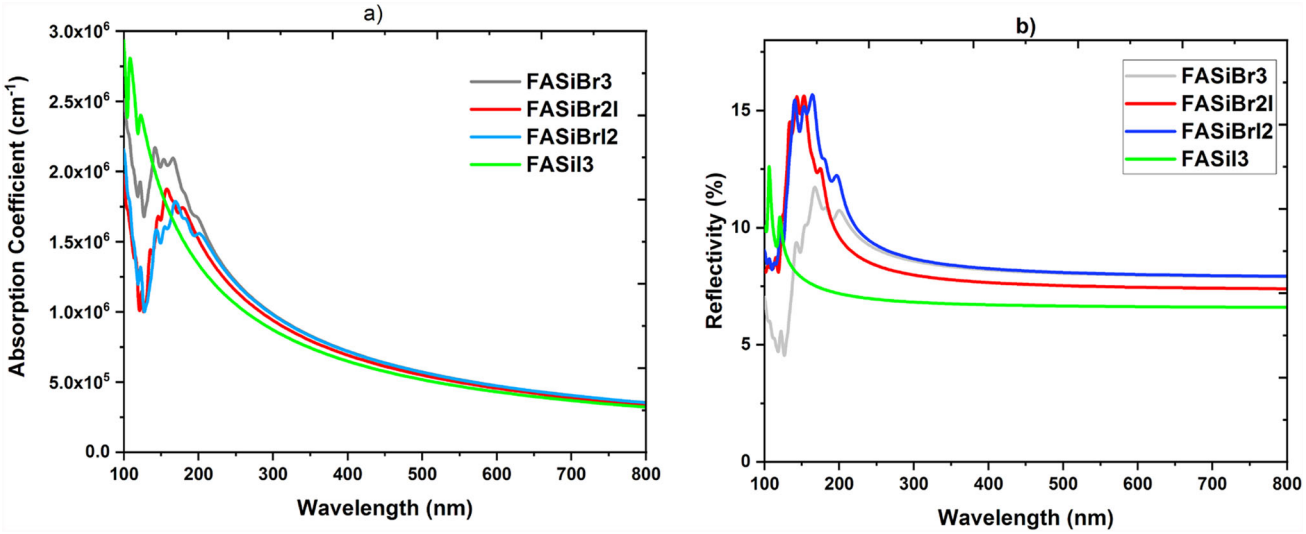


Fig. 12 In **a** the absorption coefficient and **b** the reflectivity of $FASiBr_{3-X}I_X$ ($X = 0$, 1, 2 or 3)

can vary significantly depending on surface shape, crystal positions, and composition. In addition, the wavelength and incidence angle of the incident photons may have an impact on the $FASiX_3$ perovskite reflectivity. The reflectivity has been illustrated in Fig. 12b, one can notice that a great Amount of solar energy reflected significantly in the ultraviolet-range, when excited radiation wavelength increases, reflectivity increases, and reaches a highest peak at around 15.44% at wavelength 166.14 nm for $FASiBrI_2$. The obtained reflectivity demonstrates that these materials have a high optical absorption capability. However, more research effort should be done to decrease reflectivity in the visible-energy region, which could increase absorption mechanism and enhance the performance of PSCs.

In addition, a detailed stability investigation of our considered compound $FASiX_3$ remains unrevealed. Moreover, the chemical, mechanical, and dynamical stability properties of this Silicon-based perovskite have not been previously calculated and are yet to be explored further, in order to integrate this material in photovoltaic solar cell applications.

Moreover, the effect of including the SOC on the band gap has been inspected. It is demonstrated that the band gap reduces when adding the SOC correction. The band gap was estimated around 2.60 eV (HSE) for $FASiBr_3$ without SOC, and decreases to reach 1.52 eV, when take into account the SOC effect. Further, the optical behavior of $FASiBr_{3-X}I_X$ ($X = 0$, 1, 2 or 3) has been presented; the $FASiBr_3$ was not capable of absorbing effectively the light of the solar spectrum because of its large band gap. The substitution of Br with I atom in $FASiI_3$ can enhance the absorption. Thus, may be a potential candidate to free-lead perovskite for photovoltaic cells.

4 Conclusion

In this study, the structural and optoelectronic properties of the $FASiBr_{3-X}I_X$ ($X = 0$, 1, 2 or 3) perovskite have been explored using Quantum Espresso to performs both the DFT and TDDFT methods. The band structure, DOS and PDOS of these perovskites have been calculated and discussed. The electronic properties analysis shows that the substitution of Br with I could considerably reduce the band gap of $FASiBr_3$. In particular, the band structure demonstrates that the Pb-free $FASiBr_3$ $FASiBr_2I$, $FASiBrI_2$ and $FASiI_3$ have a semiconductor nature with a direct band gap of (2.09 eV) (2.60 eV) PBE(HSE), (1.90 eV) (2.38 eV) PBE(HSE), (1.71 eV) (2.12 eV) PBE(HSE) and 1.60 eV (2.08) PBE(HSE), respectively, which indicates that these absorber materials are appropriate to make perovskite solar cells. In addition, the primary contributor was identified to be the orbital of Si, Br and I atoms, as demonstrated by the DOS analysis.

Acknowledgements The computing tool and the technical support applied for this simulation have been provided by CRESCO HP/ENEAGRID, the Italian National Agency for New Technologies [65]. The computations have been performed on CRESCO, High Performance Computing infrastructure [66] under the VIPERLAB financial support from the European Union's Horizon 2020 research and innovation program (Grant N°101006715).

Author contributions

All authors contributed equally to this work.

Funding Open access funding provided by the Carolinas Consortium.

Data availability The data that support the findings of this study are available on request from the corresponding author.

Declarations

Conflict of interest The authors have no competing interests to declare.

Open Access This article is licensed under a Creative Commons Attribution 4.0 International License, which permits use, sharing, adaptation, distribution and reproduction in any medium or format, as long as you give appropriate credit to the original author(s) and the source, provide a link to the Creative Commons licence, and indicate if changes were made. The images or other third party material in this article are included in the article's Creative Commons licence, unless indicated otherwise in a credit line to the material. If material is not included in the article's Creative Commons licence and your intended use is not permitted by statutory regulation or exceeds the permitted use, you will need to obtain permission directly from the copyright holder. To view a copy of this licence, visit http://creativecommons.org/licenses/by/4.0/.

References

1. M.K. Hossain, S. Islam, M.N. Sakib, M.S. Uddin, G.F.I. Toki, M.H.K. Rubel, J. Nasrin, S.H. Shahatha, M.R. Mohammad, A.A. Alothman, C.J. Raorane, R. Haldhar, H. Bencherif, Exploring the optoelectronic and photovoltaic characteristics of lead-free Cs2TiBr 6 double perovskite solar cells: a DFT and SCAPS-1D investigations. Adv. Electr. Mater. (2024). https://doi.org/10.1002/aelm.202400348
2. M.S. Uddin, M.K. Hossain, M.B. Uddin, G.F.I. Toki, M. Ouladsmane, M.H.K. Rubel, D.I. Tishkevich, P. Sasikumar, R. Haldhar, R. Pandey, An in-depth investigation of the combined optoelectronic and photovoltaic properties of lead-free Cs2AgBiBr 6 double perovskite solar cells using DFT and SCAPS-1D frameworks. Adv. Electron. Mater. **10**, 2300751 (2024). https://doi.org/10.1002/aelm.202300751
3. M.K.A. Mohammed, A.K. Al-Mousoi, S. Singh, A. Kumar, M.K. Hossain, S.Q. Salih, P. Sasikumar, R. Pandey, A.A. Yadav, Z.M. Yaseen, Improving the performance of perovskite solar cells with carbon nanotubes as a hole transport layer. Opt. Mater. **138**, 113702 (2023). https://doi.org/10.1016/j.optmat.2023.113702
4. M.K. Basher, M.K. Hossain, M.A.R. Akand, Effect of surface texturization on minority carrier lifetime and photovoltaic performance of monocrystalline silicon solar cell. Optik **176**, 93–101 (2019). https://doi.org/10.1016/j.ijleo.2018.09.042
5. M.K. Basher, M.K. Hossain, M.J. Uddin, M.A.R. Akand, K.M. Shorowordi, Effect of pyramidal texturization on the optical surface reflectance of monocrystalline photovoltaic silicon wafers. Optik **172**, 801–811 (2018). https://doi.org/10.1016/j.ijleo.2018.07.116
6. M.I. Hossain, W. Qarony, M.K. Hossain, M.K. Debnath, M.J. Uddin, Y.H. Tsang, Effect of back reflectors on photon absorption in thin-film amorphous silicon solar cells. Appl. Nanosci. **7**, 489–497 (2017). https://doi.org/10.1007/s13204-017-0582-y
7. M.K. Hossain, M.T. Rahman, M.K. Basher, M.J. Afzal, M.S. Bashar, Impact of ionizing radiation doses on nanocrystalline TiO_2 layer in DSSC's photoanode film. Results Phys. **11**, 1172–1181 (2018). https://doi.org/10.1016/j.rinp.2018.10.006
8. M.K. Hossain, M.T. Rahman, M.K. Basher, M.S. Manir, M.S. Bashar, Influence of thickness variation of gamma-irradiated DSSC photoanodic TiO2 film on structural, morphological and optical properties. Optik **178**, 449–460 (2019). https://doi.org/10.1016/j.ijleo.2018.09.170
9. Best Research-Cell Efficiency Chart|Photovoltaic Research|NREL, (n.d.). https://www.nrel.gov/pv/cell-efficiency.html. Accessed 10 Nov 2021.
10. A. Kojima, K. Teshima, Y. Shirai, T. Miyasaka, Organometal halide perovskites as visible-light sensitizers for photovoltaic cells. J. Am. Chem. Soc. **131**, 6050–6051 (2009). https://doi.org/10.1021/ja809598r
11. S. Idrissi, H. Labrim, L. Bahmad, A. Benyoussef, DFT and TDDFT studies of the new inorganic perovskite CsPbI3 for solar cell applications. Chem. Phys. Lett. **766**, 138347 (2021). https://doi.org/10.1016/j.cplett.2021.138347
12. Q. Han, S. Bae, P. Sun, Y. Hsieh, Y. Yang, Y.S. Rim, H. Zhao, Q. Chen, W. Shi, G. Li, Y. Yang, Single crystal formamidinium lead iodide (FAPbI3): insight into the structural, optical, and electrical properties. Adv. Mater. **28**, 2253–2258 (2016). https://doi.org/10.1002/adma.201505002
13. T.M. Koh, K. Fu, Y. Fang, S. Chen, T.C. Sum, N. Mathews, S.G. Mhaisalkar, P.P. Boix, T. Baikie, Formamidinium-containing metal-halide: an alternative material for near-IR absorption perovskite solar cells. J. Phys. Chem. C **118**, 16458–16462 (2014). https://doi.org/10.1021/jp411112k
14. F. Cordero, F. Craciun, F. Trequattrini, A. Generosi, B. Paci, A.M. Paoletti, G. Pennesi, Stability of cubic $FAPbI_3$ from X-ray diffraction, anelastic, and dielectric measurements. J. Phys. Chem. Lett. **10**, 2463–2469 (2019). https://doi.org/10.1021/acs.jpclett.9b00896
15. H. Lu, Y. Liu, P. Ahlawat, A. Mishra, W.R. Tress, F.T. Eickemeyer, Y. Yang, F. Fu, Z. Wang, C.E. Avalos, B.I. Carlsen, A. Agarwalla, X. Zhang, X. Li, Y. Zhan, S.M. Zakeeruddin, L. Emsley, U. Rothlisberger, L. Zheng, A. Hagfeldt, M. Grätzel, Vapor-assisted deposition of highly efficient, stable black-phase FAPbI3 perovskite solar cells. Science **370**, eabb8985 (2020). https://doi.org/10.1126/science.abb8985
16. A.A. Zhumekenov, M.I. Saidaminov, M.A. Haque, E. Alarousu, S.P. Sarmah, B. Murali, I. Dursun, X.-H. Miao, A.L. Abdelhady, T. Wu, O.F. Mohammed, O.M. Bakr, Formamidinium lead halide perovskite crystals with unprecedented long carrier dynamics and diffusion length. ACS Energy Lett. **1**, 32–37 (2016). https://doi.org/10.1021/acsenergylett.6b00002
17. M.K. Hossain, M.K.A. Mohammed, R. Pandey, A.A. Arnab, M.H.K. Rubel, K.M. Hossain, M.H. Ali, Md.F. Rahman, H. Bencherif, J. Madan, Md.R. Islam, D.P. Samajdar, S. Bhattarai, Numerical analysis in DFT and SCAPS-1D on the influence of different charge transport layers of CsPbBr 3 perovskite solar cells. Energy Fuels

37, 6078–6098 (2023). https://doi.org/10.1021/acs.energyfuels.3c00035
18. Monika, S. Pachori, S. Kumari, A.S. Verma, An emerging high performance photovoltaic device with mechanical stability constants of hybrid (HC(NH2)2PbI3) perovskite. J. Mater. Sci. Mater. Electron. **31**, 18004–18017 (2020). https://doi.org/10.1007/s10854-020-04352-0
19. R. Mayengbam, Structural, electronic, optical and mechanical properties of Zn-doped MAPbI3 perovskites and absorber layer efficiencies—an ab-initio investigation. Mater. Today Commun. **12**, 101216 (2020)
20. Z. Zhao, F. Gu, Y. Li, W. Sun, S. Ye, H. Rao, Z. Liu, Z. Bian, C. Huang, Mixed-organic-cation tin iodide for lead-free perovskite solar cells with an efficiency of 8.12%. Adv. Sci. **4**, 1700204 (2017). https://doi.org/10.1002/advs.201700204
21. R. Jacobs, G. Luo, D. Morgan, Materials discovery of stable and nontoxic halide perovskite materials for high-efficiency solar cells. Adv. Funct. Mater. **29**, 1804354 (2019). https://doi.org/10.1002/adfm.201804354
22. Y. Dang, Y. Zhou, X. Liu, D. Ju, S. Xia, H. Xia, X. Tao, Formation of hybrid perovskite tin iodide single crystals by top-seeded solution growth. Angew. Chem. Int. Ed. Engl. **55**, 3447–3450 (2016). https://doi.org/10.1002/anie.201511792
23. F. Valadares, I. Guilhon, L.K. Teles, M. Marques, Electronic structure panorama of halide perovskites: approximated DFT-1/2 quasiparticle and relativistic corrections. J. Phys. Chem. C **124**, 18390–18400 (2020). https://doi.org/10.1021/acs.jpcc.0c03672
24. W. Pu, W. Xiao, J. Wang, X. Li, L. Wang, Screening of perovskite materials for solar cell applications by first-principles calculations. Mater. Des. **198**, 109387 (2021). https://doi.org/10.1016/j.matdes.2020.109387
25. Y. El Arfaoui, M. Khenfouch, N. Habiballah, A DFT and time-dependent DFT investigation of the structural, electronic and optical properties of lead-free FAMgI3 perovskite for photovoltaic applications. J. Electron. Mater. (2023). https://doi.org/10.1007/s11664-023-10801-3
26. Y. El Arfaoui, M. Khenfouch, N. Habiballah, DFT and SCAPS-1D calculations of FASnI3-based perovskite solar cell using ZnO as an electron transport layer. Eur. Phys. J. Appl. Phys. (2023). https://doi.org/10.1051/epjap/2023230099
27. Y.E. Arfaoui, M. Khenfouch, N. Habiballah, Efficient all lead-free perovskite solar cell simulation of FASnI3/FAGeCl3 with 30% efficiency: SCAPS-1D investigation. Results Opt. **13**, 100554 (2023)
28. Y. el Arfaoui, M. Khenfouch, N. Habiballah, HTL-free non-toxic perovskite tandem solar device MAGeI3/FASnI3 with 25.69% efficiency: design and simulation using SCAPS. J. Opt. (2024). https://doi.org/10.1007/s12596-023-01647-3
29. Y. El Arfaoui, M. Khenfouch, N. Habiballah, New narrow band gap of silicon-based perovskite FASiI3 for photovoltaic applications: first principle investigations of the structural, electronic and optical properties. Eur. Phys. J. B. **97**, 19 (2024). https://doi.org/10.1140/epjb/s10051-024-00655-x
30. Y. El Arfaoui, M. Khenfouch, N. Habiballah, Optimization of all Pb-free perovskite CsGeI3/FASnI3 tandem solar device with 30.42% efficiency: Numerical simulation using SCAPS. Optik (2024). https://doi.org/10.1016/j.ijleo.2024.171638
31. M.I. Arz, D. Geiß, M. Straßmann, G. Schnakenburg, A.C. Filippou, Silicon(I) chemistry: the NHC-stabilised silicon(I) halides Si2X2(Idipp)2 (X = Br, I) and the disilicon(I)-iodido cation [Si2(I)(Idipp)2]+. Chem. Sci. **6**, 6515–6524 (2015). https://doi.org/10.1039/C5SC02681D
32. Z. Benedek, T. Szilvási, Can low-valent silicon compounds be better transition metal ligands than phosphines and NHCs? RSC Adv. **5**, 5077–5086 (2014). https://doi.org/10.1039/C4RA14417A
33. Z. Wang, J. Zhang, J. Li, C. Cui, NHC-stabilized silicon-carbon mixed cumulene. J. Am. Chem. Soc. **138**, 10421–10424 (2016). https://doi.org/10.1021/jacs.6b06960
34. A. Amat, E. Mosconi, E. Ronca, C. Quarti, P. Umari, Md.K. Nazeeruddin, M. Grätzel, F. De Angelis, Cation-induced band-gap tuning in organohalide perovskites: interplay of spin-orbit coupling and octahedra tilting. Nano Lett. **14**, 3608–3616 (2014). https://doi.org/10.1021/nl5012992
35. W. Shockley, H.J. Queisser, Detailed balance limit of efficiency of p-n junction solar cells, (n.d.) 11.
36. R. Hawke, M. Filip, A.-A. Haghighirad, N. Sakai, B. Wenger, F. Giustino, H. Snaith, Cubic or orthorhombic? Revealing the crystal structure of metastable black-phase CsPbI 3 by theory and experiment. ACS Energy Lett. (2018). https://doi.org/10.1021/acsenergylett.8b00672
37. N. Bibi, M. Usman, R. Ruyhan, Exploration of Na-based $NaXO_3$ (X = Ge, Si) oxide-perovskites: a density functional theory study. Comput. Theor. Chem. **1240**, 114842 (2024). https://doi.org/10.1016/j.comptc.2024.114842
38. A.A. Pasha, H. Khan, M. Sohail, N. Rahman, R. Khan, O.H. Alsalmi, D. Abduvalieva, K.M. Abualnaja, A.E. Jery, M. Adrdery, Computational study of the physical characteristics of Si-based oxide perovskites for energy generation using DFT. Mater. Adv. **4**, 6645–6654 (2023). https://doi.org/10.1039/D3MA00537B
39. M. Husain, N. Rahman, A. Azzouz-Rached, V. Tirth, H. Ullah, M. Elhadi, M. Uzair, A. Alotaibi, Q. Humayun, N. Sfina, J. Lu, Exploring silicon-based Ca_2TiSiO_6 ordered double perovskite oxides: a comprehensive DFT investigation of structural, dynamical, mechanical stability, and optoelectronic properties. SILICON **16**, 2781–2790 (2024). https://doi.org/10.1007/s12633-024-02901-4
40. L. Huang, W.R.L. Lambrecht, Electronic band structure trends of perovskite halides: beyond Pb and Sn to Ge and Si. Phys. Rev. B **93**, 195211 (2016). https://doi.org/10.1103/PhysRevB.93.195211
41. P. Giannozzi, O. Andreussi, T. Brumme, O. Bunau, M.B. Nardelli, M. Calandra, R. Car, C. Cavazzoni, D. Ceresoli, M. Cococcioni, N. Colonna, I. Carnimeo, A.D. Corso, S. de Gironcoli, P. Delugas, R.A. DiStasio, A. Ferretti, A. Floris, G. Fratesi, G. Fugallo, R. Gebauer, U. Gerstmann, F. Giustino, T. Gorni, J. Jia, M. Kawamura, H.-Y. Ko, A. Kokalj, E. Küçükbenli, M. Lazzeri, M. Marsili, N. Marzari, F. Mauri, N.L. Nguyen, H.-V. Nguyen, A. Otero-de-la-Roza, L. Paulatto, S. Poncé, D.

Rocca, R. Sabatini, B. Santra, M. Schlipf, A.P. Seitsonen, A. Smogunov, I. Timrov, T. Thonhauser, P. Umari, N. Vast, X. Wu, S. Baroni, Advanced capabilities for materials modelling with quantum ESPRESSO. J. Phys. Condens. Matter **29**, 465901 (2017). https://doi.org/10.1088/1361-648X/aa8f79
42. J.P. Perdew, J.A. Chevary, S.H. Vosko, K.A. Jackson, M.R. Pederson, D.J. Singh, C. Fiolhais, Atoms, molecules, solids, and surfaces: applications of the generalized gradient approximation for exchange and correlation. Phys. Rev. B **46**, 6671–6687 (1992). https://doi.org/10.1103/PhysRevB.46.6671
43. J.P. Perdew, A. Ruzsinszky, G.I. Csonka, O.A. Vydrov, G.E. Scuseria, L.A. Constantin, X. Zhou, K. Burke, Restoring the density-gradient expansion for exchange in solids and surfaces. Phys. Rev. Lett. **100**, 136406 (2008). https://doi.org/10.1103/PhysRevLett.100.136406
44. P. Blaha, K. Schwarz, P. Sorantin, S.B. Trickey, Full-potential, linearized augmented plane wave programs for crystalline systems. Comput. Phys. Commun. **59**, 399–415 (1990). https://doi.org/10.1016/0010-4655(90)90187-6
45. D. Vanderbilt, Soft self-consistent pseudopotentials in a generalized eigenvalue formalism. Phys. Rev. B **41**, 7892–7895 (1990). https://doi.org/10.1103/PhysRevB.41.7892
46. D.R. Hamann, Norm-Conserving Pseudopotentials. Phys. Rev. Lett. **43**, 1494–1497 (1979). https://doi.org/10.1103/PhysRevLett.43.1494
47. A.D. Corso, A.M. Conte, Spin-orbit coupling with ultrasoft pseudopotentials: application to Au and Pt. Phys. Rev. B **71**, 115106 (2005). https://doi.org/10.1103/PhysRevB.71.115106
48. H.J. Monkhorst, J.D. Pack, Special points for Brillouin-zone integrations. Phys. Rev. B **13**, 5188–5192 (1976). https://doi.org/10.1103/PhysRevB.13.5188
49. T.H. Fischer, J. Almlof, General methods for geometry and wave function optimization. J. Phys. Chem. **96**, 9768–9774 (1992). https://doi.org/10.1021/j100203a036
50. M. Becker, T. Klüner, M. Wark, Formation of hybrid ABX3 perovskite compounds for solar cell application: first-principles calculations of effective ionic radii and determination of tolerance factors. Dalton Trans. **46**, 3500–3509 (2017). https://doi.org/10.1039/C6DT04796C
51. S. Lu, Q. Zhou, Y. Ouyang, Y. Guo, Q. Li, J. Wang, Accelerated discovery of stable lead-free hybrid organic-inorganic perovskites via machine learning. Nat. Commun. **9**, 3405 (2018). https://doi.org/10.1038/s41467-018-05761-w
52. T. Wu, X. Chen, J. Wang, Metal-free hybrid organic-inorganic perovskites for photovoltaics. J. Phys. Chem. Lett. **11**, 5938–5947 (2020). https://doi.org/10.1021/acs.jpclett.0c01645
53. R.K. Pingak, A.Z. Johannes, N.U.J. Hauwali, U.A. Deta, Lead-free perovskites TlGeClxBr 3–x (x=0,1,2,3) as promising materials for solar cell application: a DFT study. J. Phys. Conf. Ser. **2623**, 012002 (2023). https://doi.org/10.1088/1742-6596/2623/1/012002
54. A.Y. Al-Reyahi, A. Mufleh, S.M. Al Azar, M. Maghrabi, N. Al Aqtash, S.S. Essaoud, K. Berarma, A. Shaheen, M.E. Ketfi, A.A. Mousa, Exploring the physical properties of cubic CsGeBr 3-nIn (n = 0, 1, 2, 3) compounds: ab initio calculations of perovskites prospective for the application in solar cells. Solid State Sci. **148**, 107435 (2024). https://doi.org/10.1016/j.solidstatesciences.2023.107435
55. R. Rajeswarapalanichamy, A. Amudhavalli, R. Padmavathy, K. Iyakutti, Band gap engineering in halide cubic perovskites CsPbBr 3−yIy (y = 0, 1, 2, 3)—a DFT study. Mater. Sci. Eng. B **258**, 114560 (2020). https://doi.org/10.1016/j.mseb.2020.114560
56. A. Najim, B. Hartiti, H. Absike, H.J. Tchognia Nkuissi, H. Labrim, S. Fadili, P. Thevenin, M. Ertugrul, Theoretical investigation of structural, electronic, and optical properties of halide cubic perovskite CsPbBr 3-xIx. Mater. Sci. Semicond. Process. **141**, 106442 (2022). https://doi.org/10.1016/j.mssp.2021.106442
57. M.R. Filip, F. Giustino, Computational screening of homovalent lead substitution in organic-inorganic halide perovskites. J. Phys. Chem. C **120**, 166–173 (2016). https://doi.org/10.1021/acs.jpcc.5b11845
58. A. Nyayban, S. Panda, A. Chowdhury, The effect of B-site alloying on the electronic and opto-electronic properties of RbPbI3: a DFT study. Phys. B Condens. Matter **649**, 414384 (2023). https://doi.org/10.1016/j.physb.2022.414384
59. U.-G. Jong, C.-J. Yu, Y.-S. Kim, Y.-H. Kye, C.-H. Kim, First-principles study on the electronic and optical properties of inorganic perovskite Rb1-xCsxPbI3 for solar cell applications. Phys. Rev. B **98**, 125116 (2018). https://doi.org/10.1103/PhysRevB.98.125116
60. W. Shockley, H.J. Queisser, Detailed balance limit of efficiency of p-n junction solar cells. J. Appl. Phys. **32**, 510–519 (1961). https://doi.org/10.1063/1.1736034
61. D.C. Hutchings, M. Sheik-Bahae, D.J. Hagan, E.W. Van Stryland, Kramers-Krönig relations in nonlinear optics. Opt. Quant. Electron. **24**, 1–30 (1992). https://doi.org/10.1007/BF01234275
62. X. Liu, B. Xie, C. Duan, Z. Wang, B. Fan, K. Zhang, B. Lin, F.J.M. Colberts, W. Ma, R.A.J. Janssen, F. Huang, Y. Cao, A high dielectric constant non-fullerene acceptor for efficient bulk-heterojunction organic solar cells. J. Mater. Chem. A **6**, 395–403 (2018). https://doi.org/10.1039/C7TA10136H
63. J. Islam, A.K.M.A. Hossain, Narrowing band gap and enhanced visible-light absorption of metal-doped non-toxic $CsSnCl_3$ metal halides for potential optoelectronic applications. RSC Adv. **10**, 7817–7827 (2020). https://doi.org/10.1039/C9RA10407K
64. L. Peng, W. Xie, Theoretical and experimental investigations on the bulk photovoltaic effect in lead-free perovskites $MASnI_3$ and $FASnI_3$. RSC Adv. **10**, 14679–14688 (2020). https://doi.org/10.1039/D0RA02584D
65. F. Iannone, F. Ambrosino, G. Bracco, M. De Rosa, A. Funel, G. Guarnieri, S. Migliori, F. Palombi, G. Ponti, G. Santomauro, P. Procacci, CRESCO ENEA HPC clusters: a working example of a multifabric GPFS Spectrum Scale layout. In: 2019 Int. Conf. High Perform. Comput. Simul. HPCS, IEEE, Dublin, Ireland, pp. 1051–1052 (2019). https://doi.org/10.1109/HPCS48598.2019.9188135

66. A. Mariano, G. D'Amato, F. Ambrosino, G. Aprea, F. Buonocore, M. Celino, A. Colavincenzo, M. Fina, A. Funel, S. Giusepponi, G. Guarnieri, F. Palombi, S. Pierattini, G. Ponti, G. Santomauro, G. Bracco, S. Migliori, Fast Access to Remote Objects 2.0 a renewed gateway to ENEAGRID distributed computing resources. Future Gener Comput. Syst. **94**, 920–928 (2019). https://doi.org/10.1016/j.future.2017.11.032